SUPPORTING INFORMATION

Counterion condensation or lack of solvation? Understanding the activity of ions in thin film block copolymer electrolytes

Qi Lei[a], Ke Li[b], Deepra Bhattacharya[a], Jingya Xiao[a], Subarna Kole[a], Qingteng Zhang[c], Joseph Strzalka[c], Jimmy Lawrence[a], Revati Kumar[b], and Christopher G. Arges[a*]*

[a]Cain Department of Chemical Engineering, Louisiana State University, Baton Rouge, LA 70803
[b]Department of Chemistry, Louisiana State University, Baton Rouge, LA 70803
[c]X-ray Sciences Division, Argonne National Laboratory, Lemont, IL 60049

*Corresponding author: carges@lsu.edu, kumar@lsu.edu

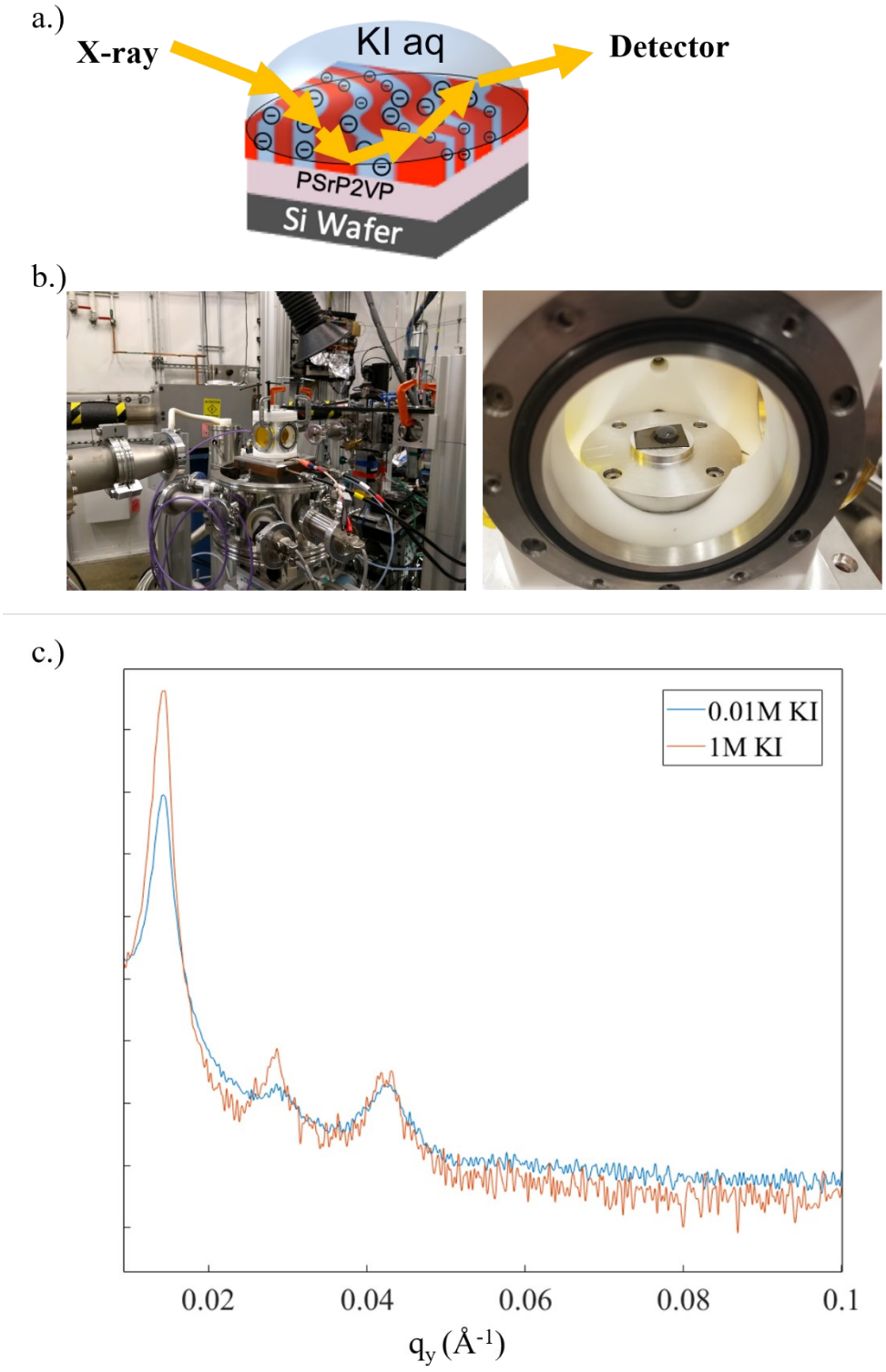

Figure S1. a.) GI-SAXS through the liquid droplet to probe a BCE thin film and b.) the experimental setup for environmental GI-SAXS at Sector 8 of the Advanced Photon Source at Argonne National Laboratory. c.) Line cuts of 2D scattering pattern of BCE film with a liquid droplet on it with two different types of KI_{aq} concentrations. Two Bragg diffraction scattering peaks were identified despite attenuation of the x-rays by the liquid droplet.

a.)

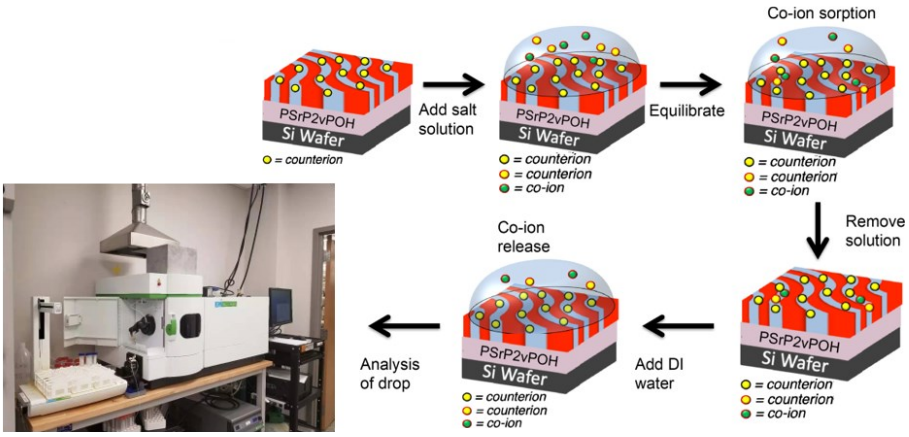

b.)

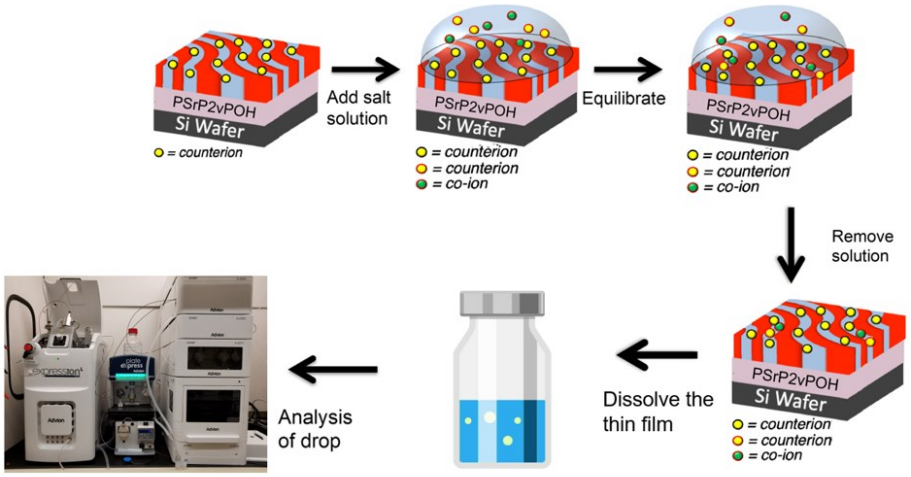

c.)

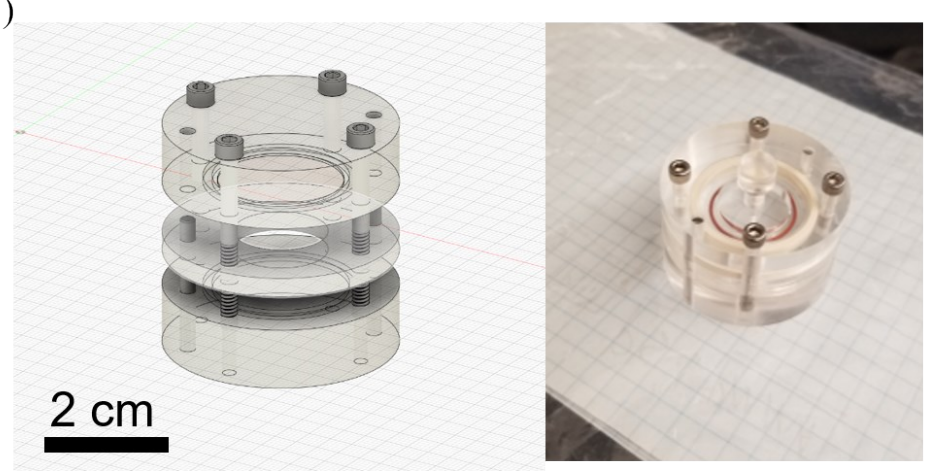

Figure S2. a.) Illustrated co-ion sorption procedure for quantifying co-ion concentration, K^+, in BCE thin films using ICP-OES b.) Illustrated procedure for assaying counterion concentration, I^-, in BCE thin films using LCMS; c) The design file and photo of ion sorption chamber.

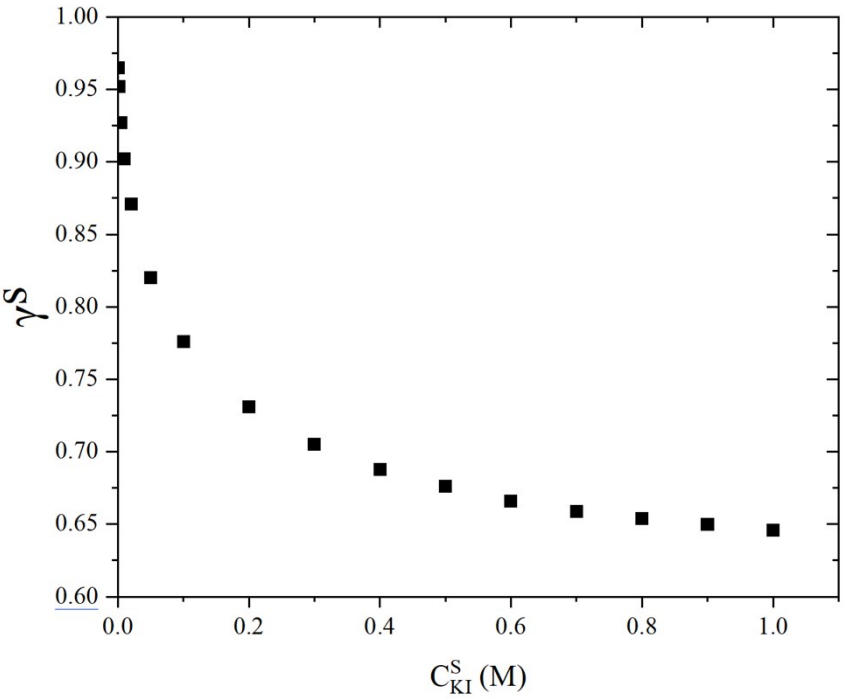

Figure S3. The mean activity coefficient values ($\gamma_{\pm}^{S}$) of KI in water attained from the literature(1).

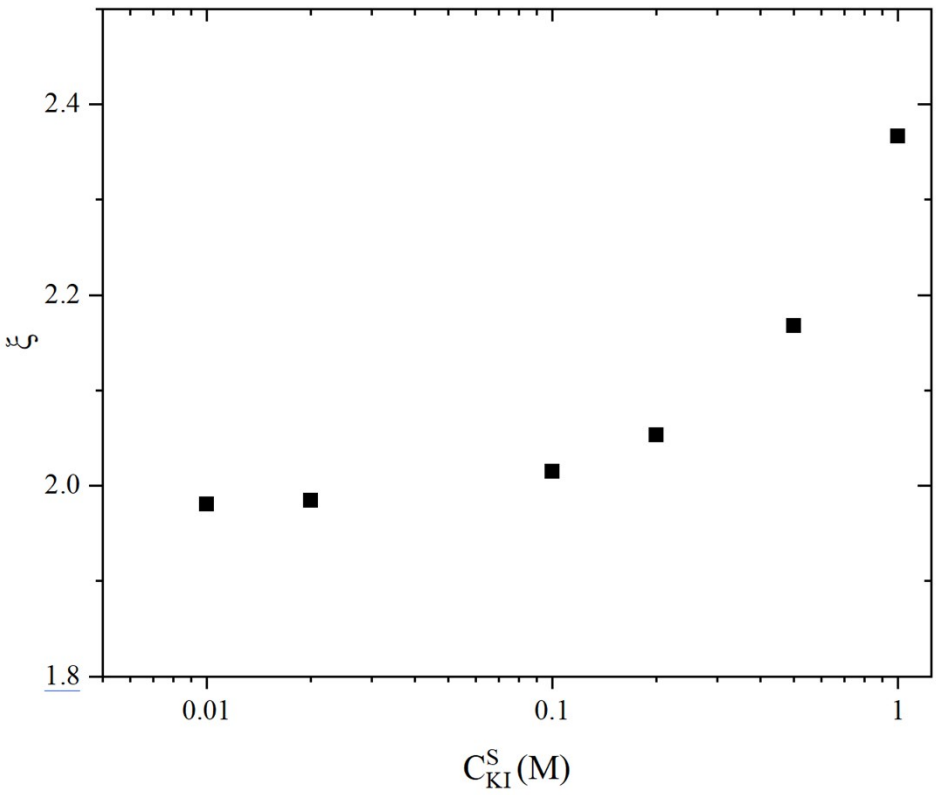

Figure S4. The Manning parameter, ξ, calculated for the BCE film interfaced with different KI_{aq} solutions. The ξ changed because ε shifted due to different solution uptake values. **Equation S1** (2) is used to determine 'b' for calculating the Manning parameter in **equation 6** in the main manuscript.

$$b = \left(\frac{n_{nc}}{n_{P2VP-NMP}} + 1\right) \times 0.252\ nm \qquad \text{<S1>}$$

n_{nc} is number of non-charged pyridine and/or styrene groups, and $n_{P2VP-NMP}$ is the number of pyridinium groups. The average length of C-C bond in PS and P2VP units was 0.126 nm. Thus, the average distance from one unit to the next unit is 0.252 nm.

Concentration dependence of static permittivity ε of electrolyte solutions, ε^{DI} = 78.36, C_S is molar concentration of salt (mol L^{-1})(3).

$$\varepsilon^S = \varepsilon^{DI} - 17.0C_S + 3.43C_S^{3/2} \qquad \text{<S2a>}$$

$$\varepsilon = f^S\varepsilon^S + f^{BCE}\varepsilon^{BCE} \qquad \text{<S2b>}$$

in which f^S and f^{BCE} are the volume fraction values of solution and BCE. ε^{BCE} is the static permittivity of BCEs. ε^{BCE} = 2 based on the literature(4).

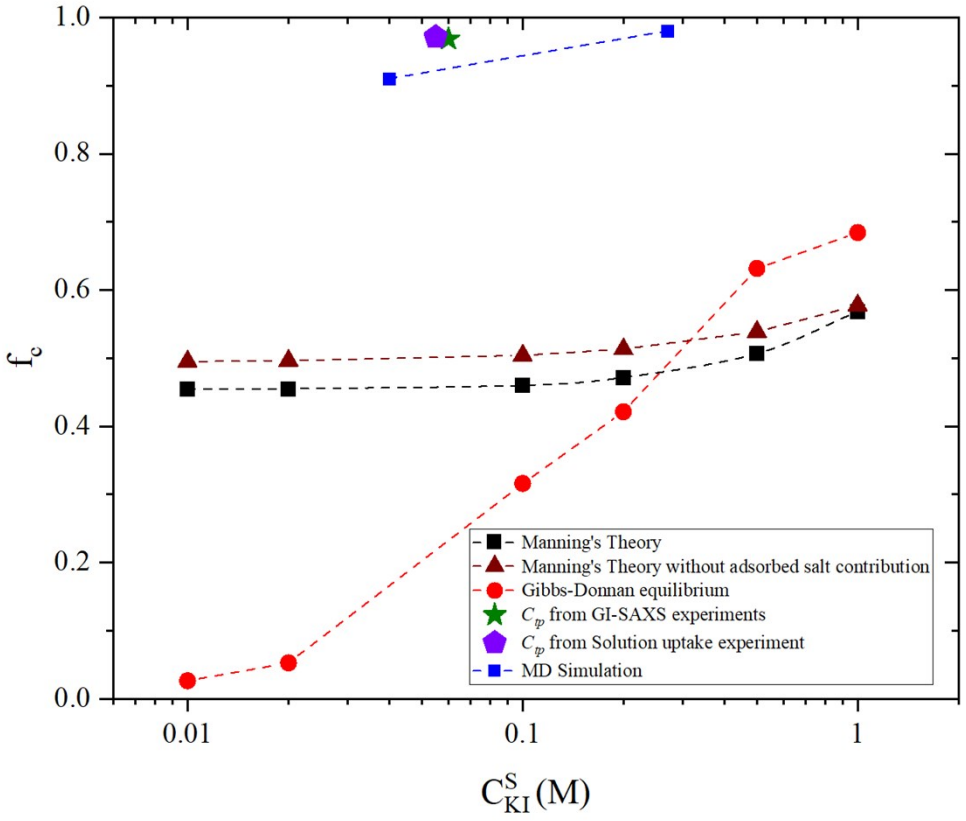

Figure S5. The f_c determined from experiments, MD simulation, and Manning's Theory of counterion condensation. Two versions of Manning's Theory are presented: one version includes the counterion contribution from the adsorbed salt and the other does not include that contribution.

$$f_c = 1 - \frac{\frac{C_{IEC}}{\xi}}{C_{IEC}} \qquad \text{<S3>}$$

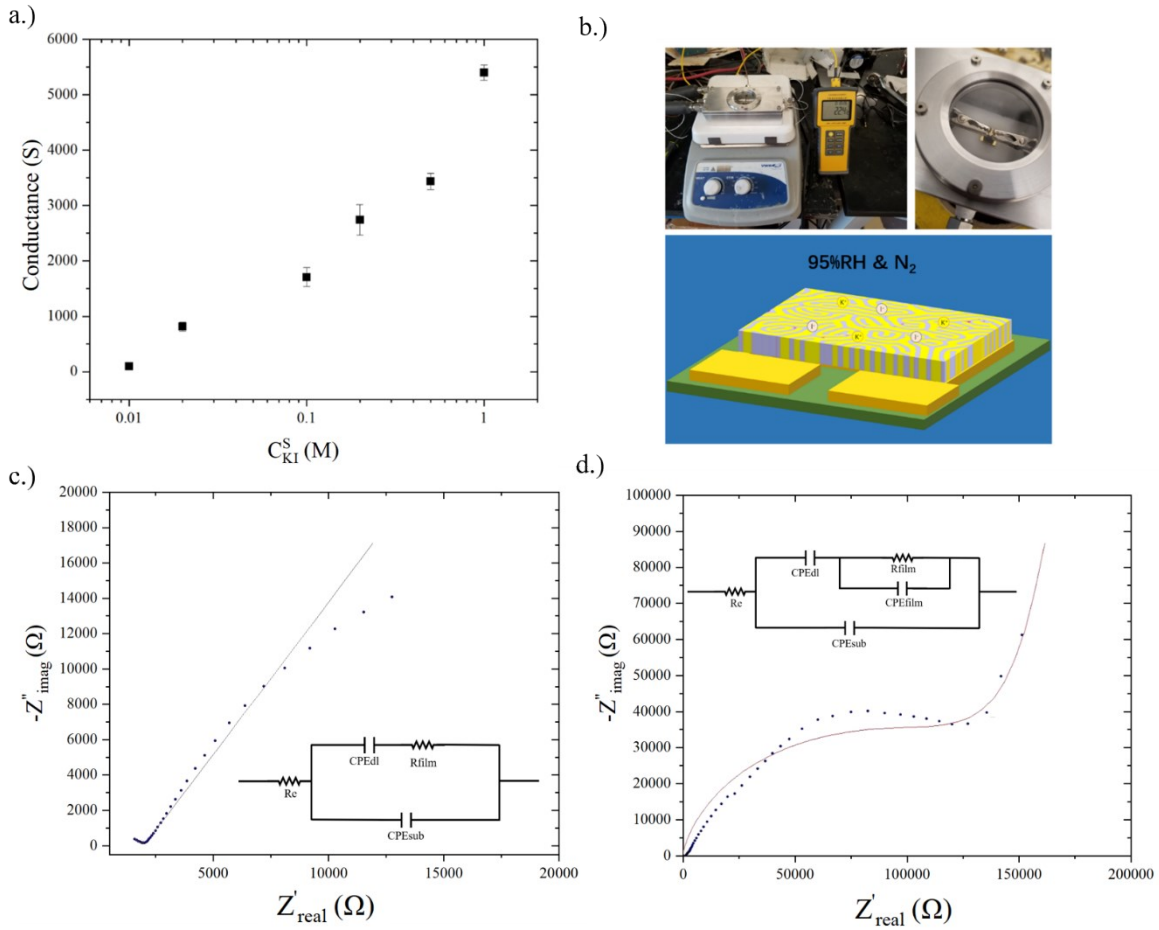

Figure S6. a.) Experimental setup for ionic conductivity experiments under 95% RH with and without liquid droplets. The experiments with the liquid droplet are carried out under humidity to prevent the droplet from evaporating; b.) The conductance of KI_{aq} droplet on bare IDEs (i.e., no BCE thin films); c.-d.) Representative Nyquist plots with ECE models fitted for BCE ionic conductivity measurements using EIS with liquid droplets (e.g., 0.1 M KI_{aq}) and 95% RH after being interfaced with 0.1 M KI_{aq}.

Ionic conductivity measurements

The Gamry Ref Potentiostat/Galvanostat with a frequency response analyzer executed the EIS experiments. The frequency range for EIS was set from 100,000 Hz to 0.1 Hz with an amplitude of 10 mA. An electric circuit equivalent (ECE) model (**Figure S6** and **equation S4**), previously described by Arges *et al.*(5), was used to interpret the impedance data and calculated the BCE film resistance. Note: The electrode pad areas of the IDE substrate were scraped away using a cotton Q-tip to remove the film for electrical connections.

$$\sigma = \frac{d}{R_{film} \cdot (n-1) \cdot l \cdot \eta_{film}} \qquad \text{<S4>}$$

R_{film} - resistance of BCEs thin film
η_{film} - thickness of BCEs thin film
d – distance between teeth on IDEs
n – number of teeth on IDEs
l – length of the teeth on IDEs

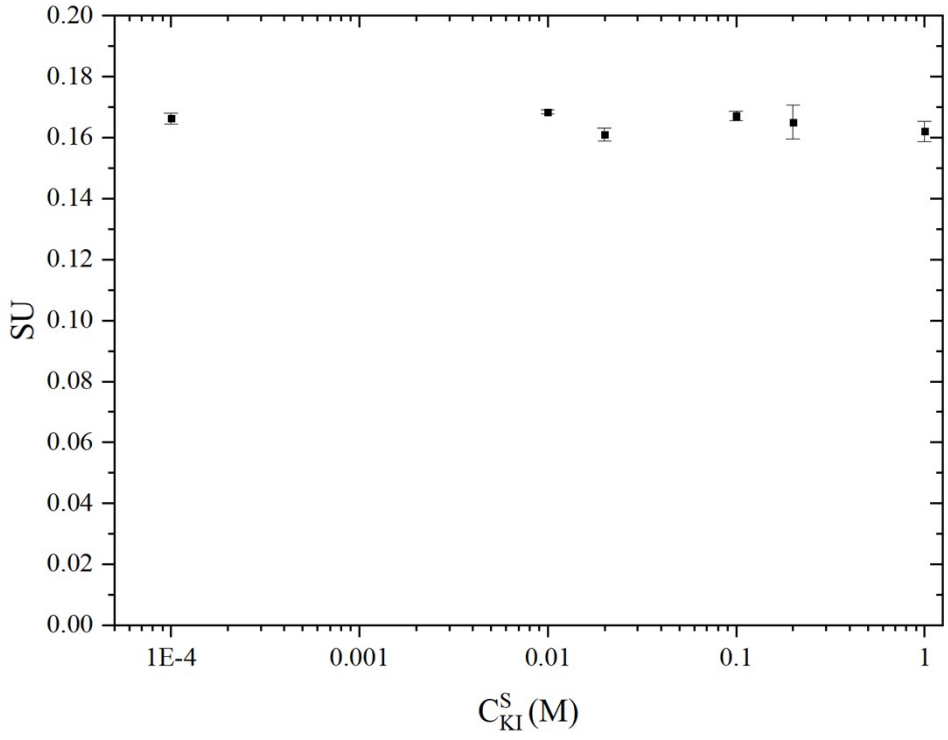

Figure S7. SU of BCEs thin film under 95% RH after being interfaced with KI_{aq}.

Table S1. Self-diffusion coefficient, conductivity and hopping rate from equilibrium simulations and from non-equilibrium simulations (with an electric field of 0.1V $Å^{-1}$) of the I^- and K^+ for: Concentrated aqueous solution of BCE without added salt, with added salt [6 molecules, 40 molecules and 90 molecules of KI corresponding to experimental solutions of 0.04 M, 0.27 M and 0.61 M)] as well as dilute BCE solution with no added salt.

	BCE	BCE (6 KI)	BCE (40 KI)	BCE (90 KI)	BCE (dilute)
I^- diffusion coefficient ($Å^2$ ns^{-1})	1.68 ± 0.02	1.92 ± 0.03	2.08 ± 0.03	3.24 ± 0.04	295.12 ± 3.59
K^+ diffusion coefficient ($Å^2$ ns^{-1})	NA	3.16 ± 0.05	4.98 ± 0.03	9.12 ± 0.09	NA
I^- conductivity (mS cm^{-1}) from Nernst-Einstein equation	1.12	1.29	1.54	2.71	8.7
K^+ Conductivity (mS cm^{-1}) from Nernst-Einstein equation	0	0.04	0.44	1.76	NA
Total Conductivity (mS cm^{-1}) from Nernst-Einstein equation	1.12	1.33	1.98	4.47	8.7
I^- conductivity from non-equilibrium simulations (mS cm^{-1})	25.9	29.4	36.5	36.8	22.4
K^+ conductivity from non-equilibrium simulations (mS cm^{-1})	NA	0.4	3.5	9.6	NA
Total conductivity from non-equilibrium simulations (mS cm^{-1})	25.9	29.8	40.0	46.4	22.4
I^- hopping rate (equilibrium simulations)	51.3	50.6	46.0	43.8	23.7
I^- hopping rate (non-equilibrium simulations)	85.9	88.8	93.2	90.2	21.58

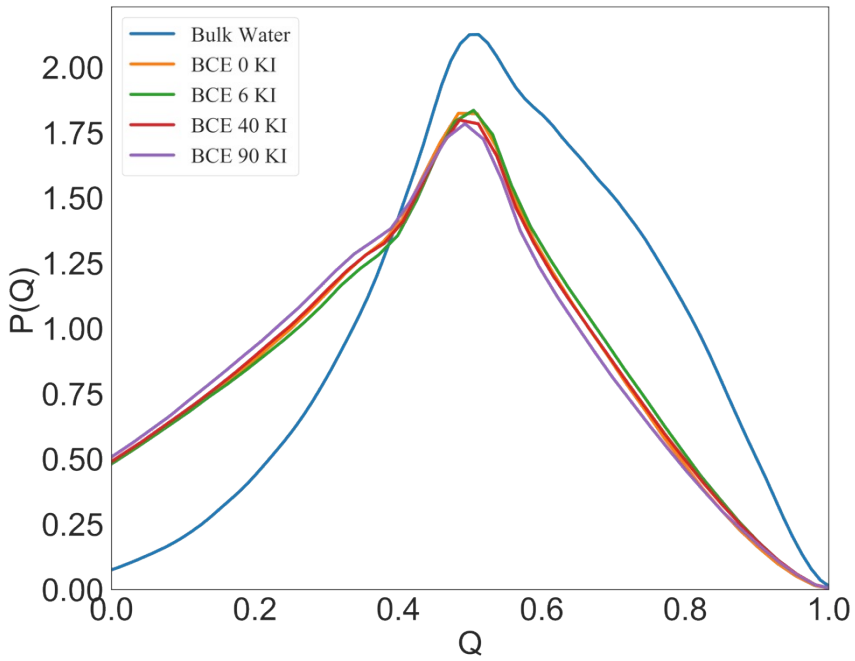

Figure S8. The probability distribution, P(Q), of the tetrahedral water order parameter, Q, for water in BCE without added salt, concentrated aqueous solution of BCE with added salt (from 6 to 90 molecules of added KI) and bulk water.

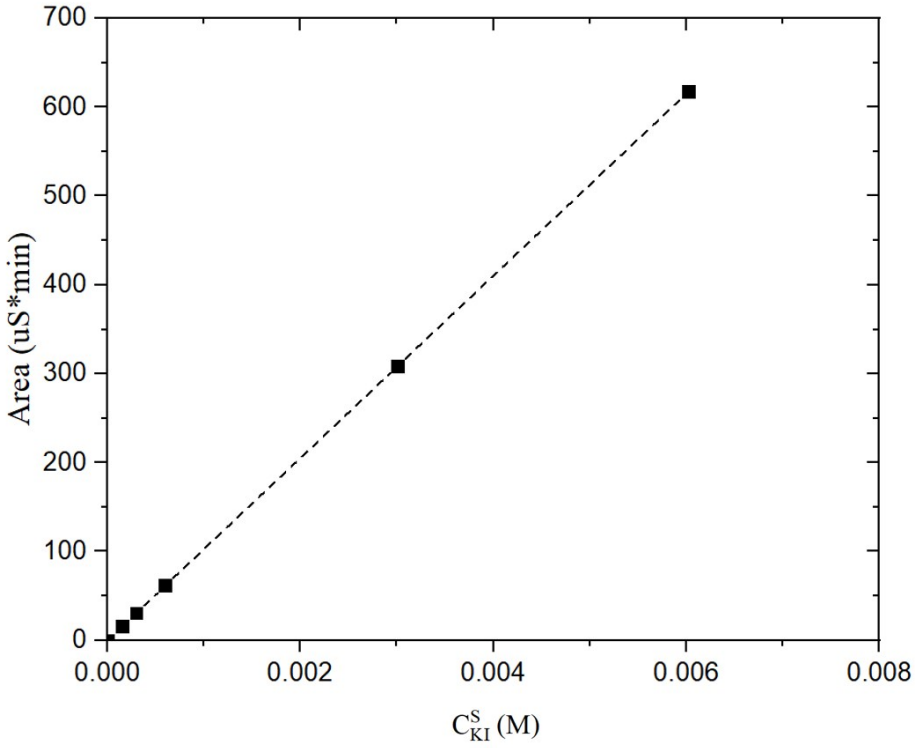

Figure S9. The calibration curve relating ICP-OES detector response to the concentration of potassium ions in aqueous solution

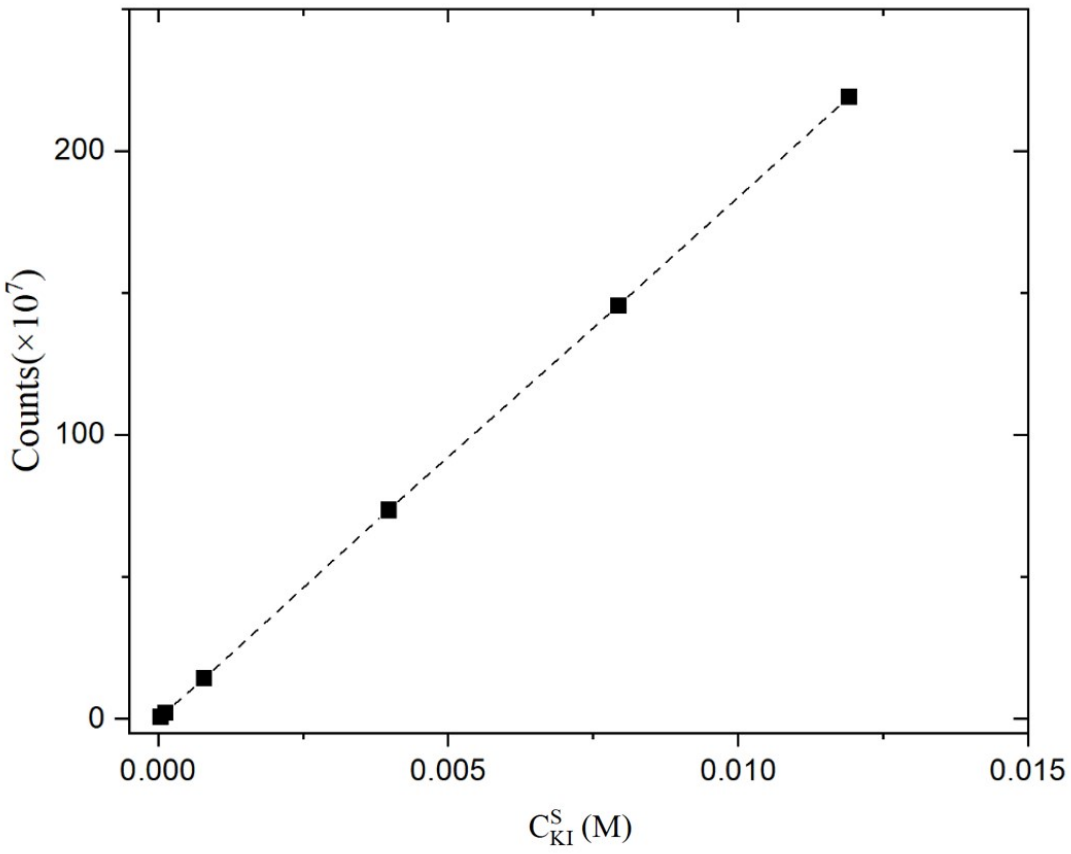

Figure S10. The calibration curve of iodide ions in aqueous solution using LCMS

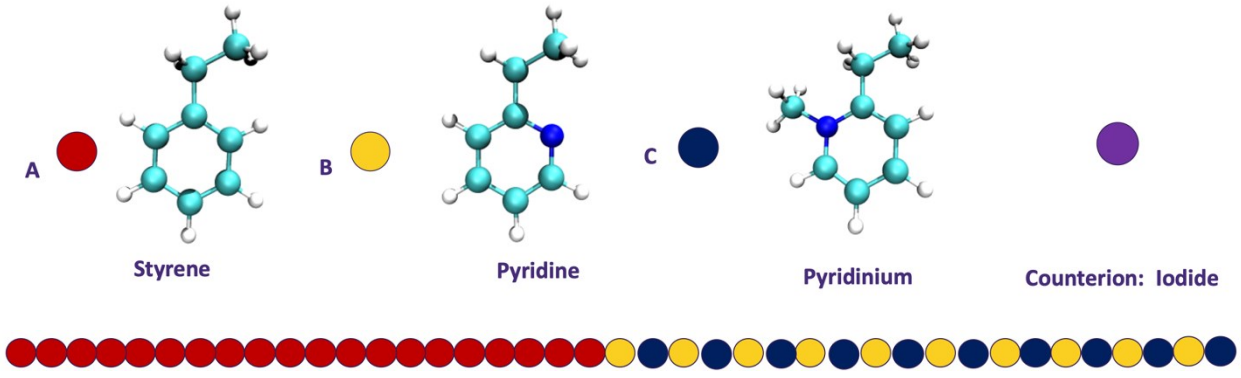

Figure S11. The model BCE with the different chemical groups.

OTHER EXPERIMENTAL METHODS

Materials

Poly (styrene-*block*-2-vinyl pyridine) (PS*b*P2VP) AB diblock copolymer sample (M_n: 40 kDa – 44 kDa) was purchased from Polymer Source Inc and used as received. Styrene (Sty), 2-vinyl pyridine (2VP), RAFT chain transfer agent (4-cyano-4-[(dodecylsulfanylthiocarbonyl)sulfanyl]pentanol), and azobisisobutyronitrile (AIBN) were purchased from Sigma-Aldrich and used as is unless specified. AIBN was recrystallized from methanol. The other chemicals, toluene, acetone, iodomethane, sulfuric acid, hydrogen peroxide, and potassium iodide were received from VWR without further purification. Two types of silicon wafers were used as substrates in this work: 1 μm thick thermally grown oxide layer of silica (SiO_x) on silicon wafers for IDEs from WRS materials and 1-inch diameter silicon wafers from University Wafer for all other experimental characterization. The gold and titanium used for thermal evaporation was received from ACI Alloys with over 99.99% purity.

Polymer characterization

Nuclear magnetic resonance (NMR) spectra were recorded on a Bruker AVIII 500 MHz spectrometer equipped with liquid nitrogen cooled Prodigy ($^1H/^{13}C/^{15}N$) probe. Size exclusion chromatography (SEC or GPC) for molecular weight analysis relative to linear polystyrene standards, was performed on a TOSOH EcoSEC Elite GPC system equipped with a refractive index detector, using THF as eluent at a flow rate of 1 mL min^{-1}.

Synthesis of hydroxyl terminated poly(styrene-r-2-vinylpyridine) (OH-PSrP2VP)

For the RAFT polymerization, the inhibitors in the Sty and 2VP monomers were removed by passing the monomer solutions through basic alumina column. These comonomers were then copolymerized using 4-cyano-4-[(dodecylsulfanylthiocarbonyl) sulfanyl]pentanol(6) (RAFT chain transfer agent) and azobisisobutyronitrile initiator (AIBN) ([Sty]:[2VP]:[CTA]:[AIBN] = 75: 25: 1: 0.2). The mixture was degassed by Ar bubbling and heated at 72 °C for 16 h. The crude polymer was diluted with chloroform, precipitated in cold hexane to remove excess monomer, and filtered to obtain the product (370 mg, isolated yield: 71%) as light orange powder ($M_{n,\,SEC}$ = 7.1 kDa, $Đ$ = 1.08, **Figure S12a**). The narrow dispersity seen in the SEC trace confirmed that the polymerization was well-controlled throughout the reaction. ^{1}H NMR analysis shows that the degree of polymerization of the random copolymer is ~80, with the styrene composition being ~70% (**Figure S12b**).

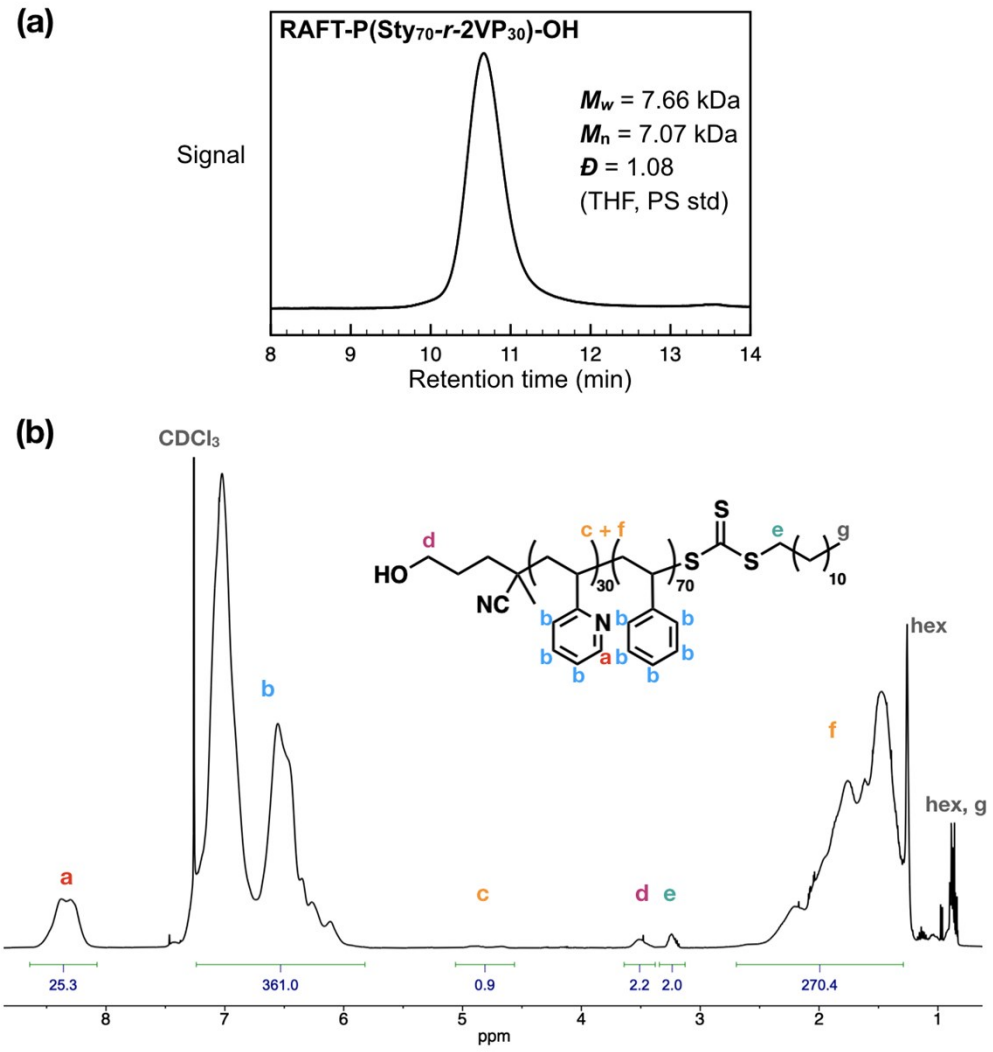

Figure S12. (a) SEC trace of OH-PS*r*P2VP. (b) ^{1}H NMR spectra ($CDCl_3$, 500 MHz) of OH-PS*r*P2VP.

Fabrication of IDEs

The procedure by Arges *et al.*(5) was followed to manufacture IDEs for thin film ionic conductivity measurements. S1813 photoresist (Microchem) was spincoated on to silicon wafers with a 1 μm thick thermally grown oxide layer (SiO_x wafers were received from WRS Materials). The photoresist coated wafer was baked at 115 °C and then placed into a mask aligner with a chromium mask of the IDE design and the resist was exposed to 225 mJ cm^{-2} of UV light. After the exposure, the wafer was developed by immersion in MF-

319 (Microchem) developer for 30 seconds with gentle shaking followed by quenching in excess deionized water. Then, 15 nm titanium was thermally evaporated on to the patterned wafers followed by 135 nm of gold. The remainder of the resist on the wafer substrates was lifted-off by immersing in acetone and placing in a sonication bath for 5 minutes. The acetone was then replaced, and the immersed wafer was then placed in the sonication bath again for 5 minutes. Afterwards, the wafer was immersed in NMP (>99.0%) solvent at 60 °C for 5 minutes. The resulting IDEs were rinsed excessively with deionized water and then dried with nitrogen. The dimensions of the IDE were 8 mm long teeth with 100 μm spacing between teeth and 100 μm wide teeth. Each IDE had 22 teeth pairs that were connected to two electrode pads.

BCP self-assembly and introduction of ionic groups post-assembly

The procedure developed by Arges *et al.*(5, 7) was used for preparing self-assembled samples of thin film BCEs composed of PS*b*P2VP/NMP^+ I^-. First, a 1 wt% solution of OH-PS*r*P2VP (70% styrene) in toluene was prepared and spin coated on the silicon wafer at 4000 rpm for 45 seconds. Then, the sample was then placed in a nitrogen gas filled chamber with a hot plate set to 200 °C for 10 minutes. At this temperature, the random copolymer was grafted to the oxide/native oxide layer of the wafers' surface. After grafting the polymer brush, the wafer was cooled and immersed in toluene under sonication to remove unreacted polymer brush. The toluene rinse step was repeated two more times to remove residual brush. Then, the wafer with grafted polymer brush was dried with nitrogen gas.

A 2 wt% solution of PS*b*P2vP diblock copolymer (M_n: 40 kDa – 44 kDa) was spin coated on the substrate with the grafted brush at 4000 rpm for 45 seconds. The block copolymer was then annealed in a solvent annealing flow chamber. The conditions for annealing were 80 sccm of saturated acetone vapor mixed with 5 sccm of dry nitrogen at room temperature resulting in a swelling ratio of a polystyrene film to 35%. The dilute acetone solvent vapor was passed across the sample for 2 hours followed by immediate termination of the solvent vapor and drying the sample at 250 sccm of dry nitrogen for 5 minutes. Then, the annealed BCP samples were placed in a 100 mL jar containing an opened 2 mL vial filled halfway with methyl iodide liquid. The jar was sealed and the sample was exposed to methyl iodide vapor for 24 hours to convert the poly (2-vinyl pyridine) block into a poly (2-vinyl pyridine-*co*-2-vinyl n-methyl pyridinium iodide). The exposure to the methyl iodide vapor introduced fixed charge carriers without disruption to the nanostructure of the BCE(7). Dissolution of the BCE thin film not exposed to KI solutions with DMF showed that 0.14 of the pyridine groups were converted to n-methyl pyridinium iodide groups. The IEC of the BCE film was 0.53 mmol g^{-1} and this corresponded to a volumetric IEC of C_{IEC} =1.90 M.

Electron microscopy

BCE thin films of PS*b*P2VP/NMP^+ I^- were imaged as is under vacuum with a Quanta™ 3D Dual beam focused-ion beam scanning electron microscope instrument operated at 5 kV with field emission gun and Solid-state backscattering electron detector. The working distance ranged from 6-13 mm.

CLASSICAL MOLECULAR DYNAMICS SIMULATIONS

Simulation setup

Simulations were carried out using a conventional non-reactive force filed based on OPLSAA.(8) A model BCE 40-mer was chosen with a hydrophobic (styrene) segment followed by a hydrophilic segment of equal length with the hydrophilic segment consisting of alternating charged (pyridinium) and unchanged (pyridine) segments (**Figure S11**). For each tethered positively charged pyridinium moiety, an iodide counterion was introduced. Using the Avogadro software,(9) the initial structure of the BCE was generated consisting of the monomeric units arranged in a line. A short 100 ps simulation of one single chain was carried out in vacuum at a temperature of 300 K in the isothermal (NVT) ensemble in a cubic box of length 100 Å. Using the resulting structure from the previous simulation, one chain was solvated with 6500 water molecules in a cubic box with a box length 60 Å using the Packmol program(10) for the dilute case. To mimic the experimental conditions, 30 chains were solvated with water in a cubic box with a box length around 100 Å. The amount of water was based on the experimental data which is about 6 waters molecules per pyridinium unit. Four separate sets of simulations were carried, one without excess salt, the others with excess KI salt added. The amount of added KI in the latter three cases was 6, 40 and 90 molecules leading to a ratio of water to KI of 1: 300, 1: 45, 1:20, respectively. These values were based on the experiments with liquid droplets of varying concentration, 0.04 M, 0.27 M and 0.61 M, respectively. The water model applied in this study is TIP3P(11) and the SHAKE(12) algorithm was used to constrain the bond lengths and bond angles for the water molecules. After random packing, each simulation box was equilibrated in the NVT ensemble for 5 ns at a temperature of 300 K

followed by 30 ns simulation in the isothermal-isobaric ensemble (temperature of 300 K and pressure of 1 atm) via the Nose-Hoover thermostat and barostat(13, 14). To get better sampling, replica exchange MD simulations were carried out(15). For each case, the replica exchange/parallel tempering simulations were carried out with 16 replica systems equally distributed between 290 K to 365 K for 20ns. The structural data was determined using the trajectories for the 300 K replica. In order to determine dynamical data, the final structures from the parallel tempering simulations at 300K were used to carry out production runs of length 20 ns in the canonical ensemble. In addition, to obtain the conductivity of the copolymer electrolyte, non-equilibrium MD simulations were performed by adding an electric field of 0.1 V $Å^{-1}$ in the z direction for 20 ns. All of the above simulations were carried out within the LAMMPS software package(16) under periodic boundary conditions with a 1 fs time step using Ewald, specifically PPPM(17), to account for long- range electrostatics.

Electronic structure calculations

In order to determine the partial charge on the atomic sites of the polymer for use in the all atom simulation, electronic structure calculations on a single repeating unit of the polymer electrolyte were carried out in each case. In particular, charges from electrostatic potentials using a grid (CHELPG) method(18) were used to determine atomic charges by fitting to the ab initio electrostatic potential on a grid around the polymer electrolyte unit molecule. The CHELPG scheme was chosen to maintain consistency with the OPLSAA force field. All electronic structure calculations were performed at the HF/6-31G* level using the GAUSSIAN 09 software(19).

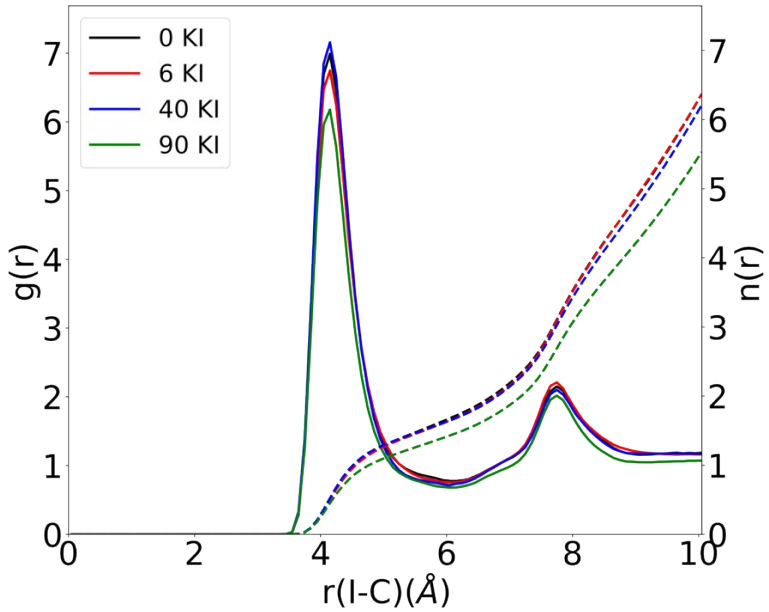

Figure S13. The radial distribution function, g(r), (solid lines) and coordination number, n(r), (dashed lines) for I-C (C from -CH_3 group attached to N) for the BCE in different salt concentrations.

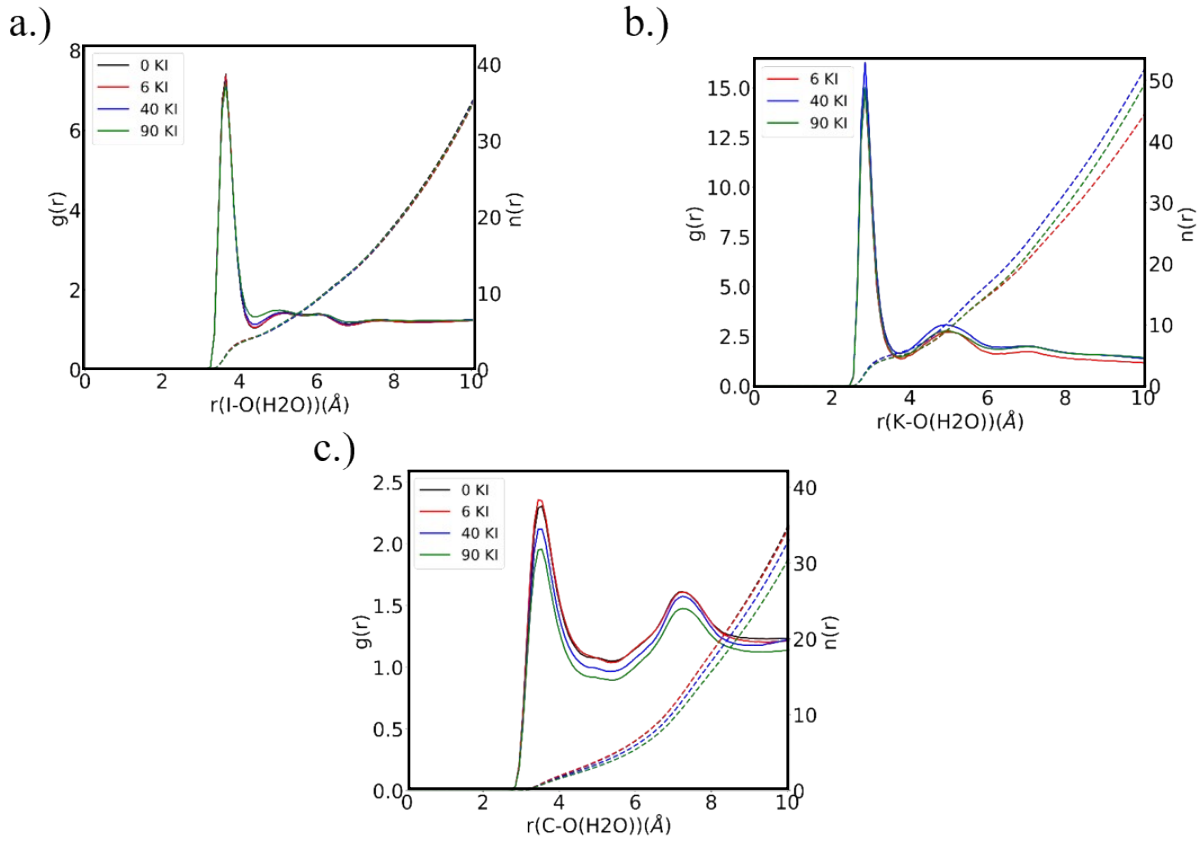

Figure S14. The radial distribution function, g(r), (solid lines) and coordination number, n(r), (dashed lines) for (a). I-O(H_2O), (b). K-O(H_2O) and (c).C (C from -CH_3 group attached to N) - O(H_2O) for the BCE in different salt concentrations.

Table S2. Ratio of the total number (N_{I-}) of condensed I^- to the total number of pyridinium units (N_C), average number of waters (n_{cw}) in first solvation shell of I^-, K^+ and pyridinium for the five cases under study

	BCE	BCE (6 KI)	BCE (40 KI)	BCE (90 KI)	BCE (dilute)
N_{I-}/N_C	0.88 ± 0.01	0.89 ± 0.01	0.99± 0.01	1.09± 0.01	0.40 ± 0.12
Coordination number for water around I^-	4.19	4.18	4.11	4.13	NA
Coordination number for water around K^+	NA	4.96	5.10	4.93	NA
Coordination number for water around pyridinium	4.66	4.60	4.24	3.84	NA

The ion-pairing of the mobile iodide counterion with the tethered charge on the polymer chain was examined using the iodide-carbon (C from -CH_3 group attached to N) radial

distribution function (see **Figure S13**). The first minimum in this radial distribution function defines the first solvation shell of pyridinium ions around an iodide ion. If the distance is less than this cutoff the iodide ion is considered to coordinated to the tethered positivity charged group of the BCE. The average fraction of iodide ions that are coordinated to the tethered positive charge for the concentrated BCE solution in the presence and absence of applied KI salt as well as for the dilute BCE solutions (excess water) in the absence of added salt are tabulated in **Table S2**. The added salt has an effect on the ratio of iodide ions that are coordinated to the tethered positive charge to the total number of pyridinium moieties, which clearly increases with the increase of salt concentration whereas the presence of excess water significantly reduces this ratio. There is no significant impact for the number of waters coordinated with I^- and K^+ with increase of salt concentration while the number of waters coordinated with pyridinium decrease with the increase of salt concentration (**Figure S14** and **Table S2**).

The effect of added salt and water on the self-diffusion of the iodide counterion was investigated. In order to do so, the mean square displacement (MSD) of the iodide ions was determined from the canonical MD simulations as follows

$$MSD = \ < D\vec{r}\,(t)^2 > \ = \frac{1}{N}\sum_{i=1}^{N}(\vec{r}_i(t) - \vec{r}_i(0))^2 \quad , \qquad \text{<S5>}$$

The self-diffusion coefficient (D) of the iodide ions can be determined from the slope (slope ~ 6D) of the linear region of the MSD as a function of time and the values are reported in **Table S1**.

Hopping rate

Hopping is considered to take place if the iodide moves from the solvation shell of one pyridinium to another. Moreover, the iodide ion has to satisfy the condition that it does not go back to the previous solvation shell in the following simulation timestep. The number of such hops during simulation divided by the product of the simulation time and number of iodides gives the hopping rate. The hopping rate for the different simulations is given in **Table S1** and is double the value in presence of the electric field as compared to the equilibrium simulations with non-applied field.

From the table it is clear that the translational dynamics of the iodide ion is significantly reduced in the low hydration regime of the experimental conditions. The conductivity (tabulated in **Table S1**) derived from the diffusion constant for the BCE using the Nernst-Einstein equation is given by (20):

$$\sigma_{NE} = \frac{e^2}{Vk_BT}\left(N_+ z_+^2 D_+ + N_- z_-^2 D_-\right), \qquad \text{<S6>}$$

where e is the elementary charge, k_B is the Boltzmann constant, V is the volume of the simulation box, and T is the temperature. $D\pm$, $z\pm$, and N± are the diffusion coefficient, charge, and number of mobile cations and mobile anions, respectively. These values are an order of magnitude smaller than the experimental conductivities. Hence, the conductivity was also directly calculated from non-equilibrium simulations with an added external electric field in the z-direction. In this case the conductivity is defined as the magnitude of the current density divided by the magnitude of electric field. The anion current *(I(t))* and conductivity *(*σ*)*are

determined from non-equilibrium simulations in the presence of an applied field, *E*, using the following equations(21)

$$I(t) = \frac{1}{dtL}\sum_{i=1}^{N} q_i[z_i(t + dt) - z_i(t))] \quad \text{<S7>}$$

where z_i is the z coordinate and q_i are the charge of atom *i*, *L* is the size of the simulation box and dt is the time interval used to record data, which was set to 2 ps. The average current, *I*, is computed by linearly fitting the cumulative current that is obtained by the integration of the instantaneous current, *I(t),* given by the above equation. The conductivity is given by

$$\sigma = \frac{I}{A \cdot E} \quad \text{<S8>}$$

where A is the area perpendicular to the field. For the concentrated BCE solution case with no added salt, the conductivity obtained from the simulation is 25.9 mS cm^{-1} which is of the same order as the experiment. The dramatic increase in the conductivity over what one would obtain from equilibrium self-diffusion data strongly indicates Grotthuss like hopping behavior of the condensed counterion.

Water structure

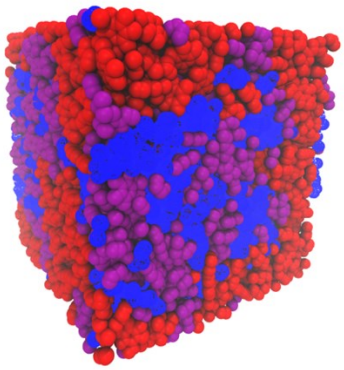

Figure S15. Simulation snapshot for BCE, purple is pyridine and pyridinium, red is styrene, blue is water Image captures the distribution of water in the MD simulations of BCEs.

The simulation trajectory of the concentrated BCE solution showed distinct water rich hydrophilic domains and water poor hydrophobic regions as is clear from the representative simulation snapshot in **Figure S15**. The tetrahedral ordering of the waters in the BCE system was quantified using the so-called tetrahedral order parameter q defined in the following manner(22).

$$q = 1 - \frac{3}{8}\sum_{j=1}^{3}\sum_{k=j+1}^{4}(cos\psi_{jik} + \frac{1}{3})^2 \qquad \text{<S9>}$$

where ψ_{jik} is the angle formed by the lines joining the central *i*th oxygen atom of a given molecule and two of its four closest heavy atom neighbors *j* and *k*. In **Figure S8** presents the distribution of this order parameter for the BCE system compared to pure bulk water. There is a clear shift to lower values of q indicating the non-bulk like solvation environment of the water in the channels. The connection between the anomalously high conductivity and the non-bulk like nature of the water channels will be examined in greater detail in future work.

Reference

1. Hamer WJ, Wu YC. Osmotic Coefficients and Mean Activity Coefficients of Uni-univalent Electrolytes in Water at 25°C. Journal of Physical and Chemical Reference Data. 1972;1(4):1047-100.
2. Kamcev J, Paul DR, Freeman BD. Ion Activity Coefficients in Ion Exchange Polymers: Applicability of Manning's Counterion Condensation Theory. Macromolecules. 2015;48(21):8011-24.
3. Shilov IY, Lyashchenko AK. Modeling activity coefficients in alkali iodide aqueous solutions using the extended Debye-Hückel theory. Journal of Molecular Liquids. 2017;240:172-8.
4. Peng J, Zawodzinski TA. Describing ion exchange membrane-electrolyte interactions for high electrolyte concentrations used in electrochemical reactors. Journal of Membrane Science. 2020;593.
5. Arges CG, Kambe Y, Dolejsi M, Wu G-P, Segal-Pertz T, Ren J, et al. Interconnected ionic domains enhance conductivity in microphase separated block copolymer electrolytes. Journal of Materials Chemistry A. 2017;5(11):5619-29.
6. Guo Y, Liu Q, Peng C, Wang E, Joy A, Cakmak M. Colloid silica nanoparticles trapped morphology of polymer blends during solvent evaporation. European Polymer Journal. 2018;107:164-72.
7. Arges CG, Kambe Y, Suh HS, Ocola LE, Nealey PF. Perpendicularly Aligned, Anion Conducting Nanochannels in Block Copolymer Electrolyte Films. Chemistry of Materials. 2016;28(5):1377-89.
8. Jorgensen WL, Maxwell DS, Tirado-Rives J. Development and testing of the OPLS all-atom force field on conformational energetics and properties of organic liquids. Journal of the American Chemical Society. 1996;118(45):11225-36.
9. López R. Capillary surfaces with free boundary in a wedge. Advances in Mathematics. 2014;262:476-83.
10. Fias S, Van Damme S, Bultinck P. Multidimensionality of delocalization indices and nucleus independent chemical shifts in polycyclic aromatic hydrocarbons. Journal of computational chemistry. 2008;29(3):358-66.
11. Jorgensen WL, Chandrasekhar J, Madura JD, Impey RW, Klein ML. Comparison of simple potential functions for simulating liquid water. The Journal of chemical physics. 1983;79(2):926-35.
12. Ryckaert J-P, Ciccotti G, Berendsen HJ. Numerical integration of the cartesian equations of motion of a system with constraints: molecular dynamics of n-alkanes. Journal of computational physics. 1977;23(3):327-41.
13. Nosé S. A unified formulation of the constant temperature molecular dynamics methods. The Journal of Chemical Physics. 1984;81(1):511-9.
14. Hoover WG. Canonical dynamics: Equilibrium phase-space distributions. Phys Rev A Gen Phys. 1985;31(3):1695-7.
15. Sugita Y, Okamoto Y. Replica-exchange molecular dynamics method for protein folding. Chemical physics letters. 1999;314(1-2):141-51.
16. Plimpton S. Fast parallel algorithms for short-range molecular dynamics. Sandia National Labs., Albuquerque, NM (United States); 1993.
17. Hockney RW, Eastwood JW. Computer simulation using particles: crc Press; 1988.

18. Breneman CM, Wiberg KB. Determining atom-centered monopoles from molecular electrostatic potentials. The need for high sampling density in formamide conformational analysis. Journal of Computational Chemistry. 1990;11(3):361-73.
19. Frisch M, Frisch M, Trucks G, Schlegel K, Scuseria G, Robb M, et al. Gaussian 03, revision D. 02. 2004.
20. France-Lanord A, Grossman JC. Correlations from ion pairing and the Nernst-Einstein equation. Physical review letters. 2019;122(13):136001.
21. Faraudo J, Calero C, Aguilella-Arzo M. Ionic partition and transport in multi-ionic channels: a molecular dynamics simulation study of the OmpF bacterial porin. Biophys J. 2010;99(7):2107-15.
22. Duboue-Dijon E, Laage D. Characterization of the Local Structure in Liquid Water by Various Order Parameters. J Phys Chem B. 2015;119(26):8406-18.